MULTIFUNCTIONAL SURFACES WITH BIOMIMETIC NANOFIBRES AND DRUG-ELUTING MICRO-PATTERNS FOR INFECTION CONTROL AND BONE TISSUE FORMATION

X.N. Chen[1], Y.X. Gu[2], J.H. Lee[2], W.Y. Lee[2] and H.J. Wang [1,*]

[1]Chemistry, Chemical Biology and Biomedical Engineering, [2]Chemical Engineering and Materials Science, Stevens Institute of Technology, Hoboken, NJ 07030, USA

Abstract

For long-term orthopaedic implants, the creation of a surface that is repulsive to bacteria while adhesive to tissue cells represents a promising strategy to control infection. To obtain such multifunctional surfaces, two possible approaches were explored to incorporate a model antibiotic, rifampicin (Rf), into the osteogenic polycaprolactone (PCL)/chitosan (CHS) biomimetic nanofibre meshes by (1) blending Rf into the electrospinning solutions and then electrospinning into nanofibres (i.e., Rf-incorporating fibres), or (2) depositing Rf-containing poly(D,L-lactic-co-glycolic) acid (PLGA) micro-patterns onto the PCL/chitosan nanofibre meshes *via* ink-jet printing (i.e., Rf-eluting micro-pattern/fibre). Rapid release of Rf from both meshes was measured even though a relatively slower release rate was obtained from the Rf-eluting micro-pattern ones. Antibacterial assay with *Staphylococcus epidermidis* showed that both mesh surfaces could effectively kill bacteria and prevent biofilm formation. However, only Rf-eluting micro-pattern meshes favoured the attachment, spreading and metabolic activity of preosteoblasts in the cell culture study. Furthermore, the Rf-eluting micro-pattern meshes could better support the osteogenic differentiation of preosteoblasts by up-regulating the gene expression of bone markers (type I collagen and alkaline phosphatase). Clearly, compared to Rf-incorporating nanofibre meshes, Rf-eluting micro-patterns could effectively prevent biofilm formation without sacrificing the osteogenic properties of PCL/chitosan nanofibre surfaces. This finding provides an innovative avenue to design multifunctional surfaces for enhancing bone tissue formation while controlling infection.

Keywords: Biomimetic nanofibres; drug-eluting micro-patterns; infection control; osteogenesis.

* Address for correspondence:
Hongjun Wang
Department of Chemistry, Chemical Biology and Biomedical Engineering,
Stevens Institute of Technology,
McLean Building Room 416,
1 Castle Point on Hudson, Hoboken, NJ 07030, USA
Telephone Number: +1 201 216 5556
FAX Number: +1 201 216 8240
E-mail: Hongjun.Wang@stevens.edu

Introduction

Infection control on abiotic surfaces remains a long-standing challenge, which becomes particularly important considering that infection is one of the leading causes of orthopaedic implant failure (Campoccia *et al.,* 2006). Continuous innovation has been made to modify material surfaces for preventing bacterial colonisation, e.g., by grafting polyethylene glycol or other hydrophilic molecules to minimise bacterial adhesion (Bearinger *et al.,* 2003; Banerjee *et al.,* 2011), or incorporating antibiotics into implant materials or coating layers for controlled release to kill bacteria (Lucke, 2003; Alt *et al.,* 2006; Radin and Ducheyne, 2007). While their efficiency in infection control has been demonstrated, there is no obvious evidence to show that these approaches would promote tissue growth. Tissue-integration with implant surface is not required for those implants for the temporary fracture fixation (Hayes *et al.,* 2009; Moriarty *et al.,* 2009; Hayes *et al.,* 2010; Moriarty *et al.,* 2010; Hayes *et al.,* 2012); however, it becomes highly crucial for long-term implants such as hip prostheses. It is recognised that the fate of long-term orthopaedic implants mainly depends on the surface race between successful osseointegration and unwanted biofilm formation (Gristina, 1987) and an ideal surface for such orthopaedic implants should be repulsive to bacteria while adhesive to bone tissue cells. Following this concept, efforts to modify the surface with differential functionality for preventing biofilm formation and promoting bone tissue formation will be of great benefit. Up to now, very limited progress has been made in designing such multifunctional surfaces. Seminal efforts were made to functionalise titanium substrates with covalently grafted chitosan, hyaluronic acid or their derivatives to suppress bacterial adhesion, while enhancing osseointegration with immobilised RGD peptides or growth factors (Shi *et al.,* 2008; Shi *et al.,* 2009; Hu *et al.,* 2010). With promising evidence in reducing bacterial adhesion and enhancing osteogenesis, the involvement of two chemical modification steps in this approach could potentially complicate its application. Thus, more cost-effective approaches are preferred.

Recently, electrospun fibre meshes have received great attention as growth substrates for various cells and tissues, due to the simple electrospinning setup and the possibility of forming fibres from a variety of polymers, and more importantly, their morphological and dimensional similarity to native extracellular matrix (ECM). The flexibility to incorporate various biomolecules into electrospun nanofibre allows the configuration of specific

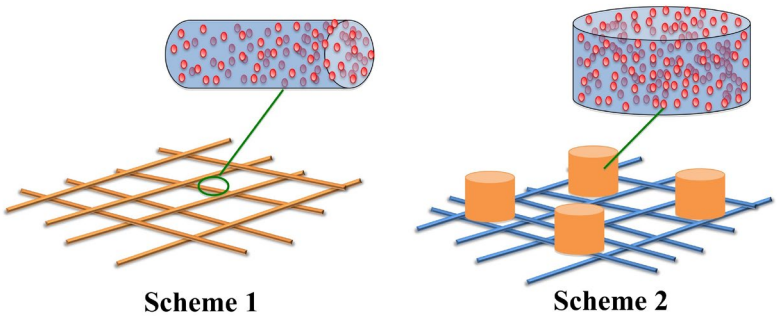

Scheme 1
Fibre-incorporated RF
(*REF*)

Scheme 2
Micro-pattern-incorporated RF
(*EFRM*)

Fig. 1. Schematic illustration of the design of multifunctional surfaces with antibacterial rifampicin (Rf) either directly incorporated in the PCL/chitosan nanofibres (fibre incorporated Rf, i.e., REF) or embedded in PLGA micro-patterns (micro-pattern incorporated Rf, i.e., EFRM). Red particles stand for Rf.

substrates for desired tissue formation. For example, blending type I collagen into polycaprolactone (PCL) fibres can significantly improve the adhesion and growth of fibroblasts for soft tissue regeneration (Venugopal *et al.,* 2006; Yang *et al.,* 2009b). Our previous study has shown that PCL/chitosan composite fibres support the adhesion and proliferation of preosteoblasts and their osteogenic differentiation (Yang *et al.,* 2009a).

In order to prevent infection, it is possible to include antifouling molecules or antimicrobial drugs into electrospun nanofibres (Kenawy *et al.,* 2002; Katti *et al.,* 2004; Kim *et al.,* 2004). With the application mainly focused on antimicrobial effects or preventing post-surgery-induced abdominal adhesions (Bölgen *et al.*, 2007; Zong *et al.*, 2004), little attention was paid to their potential effects on tissue cells. It is known that nanofibres regulate cell adhesion by interacting with various cell membrane integrins to form focal adhesion plaques as a synergistic result of both fibre morphology and surface chemistry (Schindler *et al.,* 2005; Yin *et al.,* 2010), which in turn regulate the cell phenotype (Huang *et al.*, 2012). The incorporation of such molecules in electrospun nanofibres would alter the surface properties and consequently lead to a differential cellular response. In this regard, we propose a novel strategy to introduce the antimicrobial function to electrospun nanofibre meshes while maintaining the osseointegration capacity of nanofibres. In this strategy, drug-eluting bioresorbable micro-patterns are created on the nanofibre mesh surfaces to release antimicrobial drugs that prevent bacterial colony formation. The micro-patterns can be produced with recent advances in "demand-on-drop" printing and patterning of nanocomposite materials *via* evaporative assembly, along with the significant progress in inkjet printing onto three-dimensional (3D) object surfaces with multi-axis robotics (Hamade *et al.,* 2005). Thus, the aim of this study is to demonstrate the efficacy of electrospun PCL/chitosan nanofibre meshes with antibiotic-eluting micro-patterns in preventing infection while promoting osteogenesis. The hypothesis is that antibiotics incorporated into micro-patterns would not affect the behaviour of tissue cells on nanofibre surfaces and its release can effectively kill the bacteria.

In this study, rifampicin (Rf) was used as a model antibiotic for its potency in managing bone infection and its effectiveness against *Staphylococci* (O'Reilly *et al.,* 1992; Zimmerli *et al.,* 1998). Rf is often recommended to be used in combination with other antibiotics (Zimmerli *et al.,* 2004) to achieve optimal efficacy and minimise the bacterial resistance (Shasha *et al*., 1994). However, our previous result showed that Rf alone was effective to kill planktonic *S. epidermidis* of NJ9709 strain (Lee *et al.,* 2011), which was used as the bacterium model in this study. To prove the hypothesis and achieve the multi-functionality of the multi-scale surfaces, a periodic array of poly(D,L-lactic-co-glycolic) acid (PLGA) circular patterns (~75 μm in diameter and ~150 μm apart between the centres of two adjacent micro-patterns) containing Rf were printed onto electrospun PCL/chitosan nanofibre meshes (Fig. 1). The Rf-containing PCL/chitosan nanofibre meshes (Fig. 1) were also included in the study for side-by-side comparison of the advantages of new multi-scale surfaces. The capabilities of such Rf-incorporated surfaces in killing *S. epidermidis* bacteria and supporting osteogenesis of preosteoblasts were investigated. This finding would provide us with an innovative avenue to design multifunctional surfaces for both controlling infection and enhancing bone tissue formation, which can be used to improve the surface of permanent orthopaedic implants in the near term and prevent infection in tissue-engineered grafts in the long run.

Materials and Methods

Materials

1,1,1,3,3,3-hexafluoro-2-propanol (HFIP) was obtained from Oakwood Products (West Columbia, SC, USA). Poly (ε-caprolactone) (PCL, molecular weight = 80,000) and chitosan (CHS, medium molecular weight) were purchased from Sigma-Aldrich (St. Louis, MO, USA). Dimethyl sulphoxide (DMSO, ≥ 99 %) from Sigma-Aldrich was used as a solvent for PLGA (5050DLG3E, Mw 25,000, 50 wt% PLA, Lakeshore Biomaterials, Birmingham, AL, USA) and rifampicin (Rf) (≥ 97 %, Sigma-Aldrich). Foetal bovine serum (FBS) was purchased from the American Type Culture Collection (ATCC, Manassas, VA, USA). All other reagents and solutions were obtained from Invitrogen/Life Technologies (Carlsbad, CA, USA) except as indicated.

Electrospinning and characterisation

Various nanofibres were prepared using established electrospinning techniques as described elsewhere (Yang *et al.,* 2009a). To prepare PCL/chitosan nanofibre meshes (abbreviated as *EF*), chitosan solution (0.8 wt%) and PCL solution (8 wt%) dissolved in HFIP were mixed thoroughly at a volume ratio of 1:1. These electrospun fibre (*EF*) meshes were produced at a voltage of 15 kV with a flow rate of 10 μL/min with Young's modulus as 16.0 ±1.4 MPa (Yang *et al.,* 2009a) and they were collected on square glass cover slips (22 mm × 22 mm) for both bacterial and cell culture. To prepare Rf-containing electrospun fibres (abbreviated as *REF*), Rf (0.73 wt%) was dissolved in the 1:1 (v/v) PCL/chitosan solution and mixed thoroughly prior to electrospinning. To characterise the electrospun fibres, fibres collected on silicon (Si) wafers were sputter-coated with gold and then examined with a LEO 982 field emission gun (FEG) scanning electron microscope (SEM) (Zeiss, Oberkochen, Germany). To determine the fibre diameter, images of five randomly selected areas were captured and measured by analysis software (NIS-elements BR 3.10) from Nikon (Nikon Instruments Inc., Melville, NY, USA). To measure the surface chemistry of nanofibres, Fourier transform infrared (FTIR) spectra were obtained with a Jasco (Easton, MD, USA) FT/IR-460 plus spectrometer.

Micro-pattern formation and characterisation

Rf containing PLGA circular patterns were directly printed on the 1:1 (v/v) PCL/chitosan nanofibre surface (abbreviated as *EFRM*) using a commercial inkjet printer (Dimatix Materials Printer, DMP2800, FUJIFILM Dimatix, Santa Clara, CA, USA) as described elsewhere (Gu *et al.,* 2012). The printer utilises micro-fabricated piezoelectric nozzles for on-demand and programmable generation of 10 pL droplets of jetting solutions with spatial resolution of ~50 μm. Briefly, the jetting solution was prepared by dissolving PLGA (6 wt%) and Rf (1 wt%) in DMSO at ~50 °C and stirring in the dark overnight. The prepared solution was transferred to the printer cartridge with a syringe and then ultrasonicated for 20 min. The firing voltage, nozzle temperature, substrate temperature, nozzle-substrate distance, droplet spacing, and interlayer delay for the printing were set at 30 V, 35 °C, 45 °C, 0.5 mm, 150 μm and 90 sec, respectively. 20 layers of Rf-containing micro-patterns were printed on *EF*. To characterise the morphology and size of circular micro-patterns, the collected samples were sputter-coated with gold and examined with SEM. Randomly selected images (n = 5) were used to measure the micro-pattern size and inter-pattern distance.

Release kinetics of Rf

To determine the antibiotic release, the amount of Rf per sample (n = 6) was accurately measured as 44.3 ±4.3 μg for REF and 43.7 ±3.7 μg for EFRM ($p > 0.05$), respectively. Then the samples were incubated in 2 mL phosphate buffered saline solution (PBS, pH = 7.0) at 37 °C under shaking at 50 rpm. At designated time intervals, the supernatant was collected and immediately replenished with an equal amount (2 mL) of fresh PBS in an "infinite sink" release fashion. The average Rf concentration in the collected supernatant was determined by measuring the absorbance at 330 nm (Otto *et al.,* 2008) using a Synergy™ HT multi-detection microplate reader (BioTek Instruments, Winooski, VT, USA). The UV absorbance of Rf was then converted to the concentration based on the obtained linear standard curve (Rf: 0-40 μg/mL, $r^2 > 0.997$). The measurement was performed at one-hour intervals for up to three days. The cumulative release of Rf at designated time was calculated. The percentage of total released Rf was calculated by dividing the cumulative amount of Rf in the supernatant by the total amount of Rf initially included in REF and EFRM.

Bacterial culture

Prior to testing, various substrates (EF, REF and EFRM, n = 6) collected on glass cover slips were UV sterilised for 30 min in 6-well plates. An inoculum of *S. epidermidis* biofilm strain, NJ9709, obtained from the surface of an infected intravenous catheter, was prepared as described previously (Kaplan *et al.,* 2004). The final inoculum was diluted in trypticase soy broth (TSB) medium at a final concentration of approximately 1×10^7 colony forming unit (CFU)/mL as counted by the Petroff-Hausser counting chamber (Electron Microscopy Sciences, Hatfield, PA, USA) before inoculation and confirmed by agar plating the next day. 2 mL bacterium-containing TSB medium was added to each well. After culturing for 5 hours, the supernatant from each culture was collected and planktonic bacteria in the supernatant were analysed by agar plating (n = 3). At the end of culture, half of the samples (n = 3) were stained with a live/dead fluorescent staining kit (SYTO9 green and propidium iodide: BacLight™ Bacterial Viability Kit, Invitrogen/Life Technologies) for 15 min and then examined with a Nikon Eclipse 80*i* fluorescent microscope (Nikon). The other half (n = 3) were stained with 0.75 wt% crystal violet for 5 min and then the stain was dissolved in 1 mL of 30 % acetic acid. 200 μL of the supernatant was transferred to a 96-well plate to measure the optical density (OD) using a Synergy HT multi-detection microplate reader at 595 nm.

Osteoblastic cell culture

Mouse preosteoblasts (MC 3T3-E1) from bone calvaria were cultured in α-minimum essential medium (α-MEM) supplemented with 10 % FBS, 1 % penicillin/streptomycin. The culture was maintained at 37 °C with 5 % CO_2 until 70-80 % confluence prior to use.

Cell metabolic activity

The metabolic activity of MC 3T3-E1 on various substrates (REF, EFRM, and EF) was quantified by using the 3-(4, 5-dimethylthiazol-2-yl)-2, 5-diphenyl tetrazolium bromide (MTT) assay, which can be used to reliably measure cell metabolic activity *in vitro* for assessing cell growth (Sieuwerts *et al.,* 1995). Briefly, after UV-sterilisation and medium incubation, the substrates (n = 3) were seeded with MC 3T3-E1 cells at a density of 5×10^4 cells per sample for overnight. Complete culture media (α-MEM supplemented with 10 mM β-glycerophosphate, 10^{-7} M dexamethasone

and 80 mg/mL ascorbic acid) was used to continuously culture for 1, 3 and 7 days. The culture was rinsed with PBS and then incubated with α-MEM media containing 10 % MTT solution (5 mg/mL, Sigma-Aldrich) for 2 h at 37 °C. Then the unreacted MTT solution was discarded and the metabolically formed formazan was extracted with DMSO. 200 μL of the extract was transferred to a 96-well plate and the absorbance was measured with the Synergy™ HT multi-detection microplate reader at 570 nm.

Cell morphology

After culturing for one and three days, samples were fixed in 4 % formaldehyde and permeabilised with 0.5 % Triton X-100 in PBS. The cells were stained with TRITC-conjugated-phalloidin (50 μg/mL from Sigma-Aldrich) for 40 min at room temperature and then the cell nuclei were stained with DAPI in Vectashield mounting medium (Vector Lab, Burlingame, CA, USA). Stained cells were examined with a Nikon 80*i* fluorescent microscope.

Gene expression

To compare the ability of various substrates (EF, REF and EFRM, $n = 3$) to induce the osteogenesis of preosteoblasts, reverse transcriptase polymerase chain reaction (RT-PCR) was performed on the cultured cells for marker gene expression. Total RNA was isolated using the Multisource Total RNA Miniprep Kit (Axygen Biosciences, Union City, CA, USA) and then reverse-transcribed into complementary DNA (cDNA) using the SuperScript First-Strand Synthesis System (Promega, Madison, WI, USA). The cDNA product was then amplified using recombinant Taq DNA polymerase (Promega). Expressions of type I collagen (COL-1; sense, 5′-TCTCCACTCTTCTAGTTCCT-3′; antisense, 5′-TTGGGTCATTTCCACATGC-3′, 269 bps), alkaline phosphatase (ALP; sense, 5’-GGGACTGGTACTCGGATAACGA-3’; antisense, 5’-CTGATATGCGATGTCCTTGCA-3’, 71 bps) and osteopontin (OPN; sense, 5′-ATGAGATTGGCAGTGATTTG-3′; antisense, 5′-GTAGGGACGATTGGAGTGAA -3′, 410 bps) were examined. β-actin (sense, 5’-AACCCTAAGGCCAACCGTG-3’; antisense, 5’-CAGGATTCCATACCCAAGAAG-3’, 485 bps) served as the house-keeping gene control. All genes were amplified for 30 cycles in a thermocycler (Eppendorf Mastercycler gradient, Brinkmann, Westbury, NY, USA). Semi-quantitative analysis of gene expression was performed, and band intensity was normalised to that of β-actin.

Statistical analysis

Each experiment was repeated at least 3 times on different days and data were expressed as the mean ± standard deviation (SD). All the data were collected in triplicate for each group. The nonparametric approach was applied to statistically analyse the results by using SAS (SAS Institute, Cary, NC, USA) procedure NPAR1WAY (SAS 9.2). To test if there is any difference among the three types (EF, REF and EFRM), Kruskal-Wallis test (Exact) was performed. two-sided Wilcoxon Rank Sum test (Exact) was further used to conduct pairwise comparisons. Bonferroni adjustment was used to adjust p values for multiple comparisons. A value of $p < 0.05$ was considered statistically significant.

Results

Fabrication and characterisation of biomimetic substrates

To prevent the colonisation of *S. epidermidis*, Rf, an active antibiotic was either directly incorporated into the PCL/chitosan nanofibres while electrospinning (defined as *REF* in Fig. 1) or incorporated into PLGA micro-patterns that were deposited onto the PCL/chitosan nanofibre meshes (defined as *EFRM* in Fig. 1). Table 1 shows the composition and average fibre diameter for each substrate. PCL/chitosan nanofibre meshes without Rf were included as controls and the total Rf weight percentage remained constant (14.29 %) by maintaining the weight ratio of polymer to Rf at 6 to 1 for both REF and EFRM. Due to the intrinsic red colour of Rf, both REF and PLGA micro-patterns appeared to be orange (Fig. 2b and c insets). Although the inclusion of Rf into PCL/chitosan electrospun nanofibres did not significantly change the average fibre diameter (Table 1) and fibre surface morphology (Fig. 2d and 2e insets), it caused non-uniform electrospun nanofibres as evidenced by bead formation (Fig. 2e). The surface chemistry of nanofibres was characterised by FTIR and signature peaks of Rf at approximately 1380 and 1460 cm^{-1} that corresponded to the stretching C=C bonds of naphthalene

Table 1. Formulation and dimensions of various substrates.

Material group	Composition	Dimension
EF: electrospun fibres	Electrospun PCL/chitosan nanofibrous mesh of PCL:chitosan = 10:1 = 4 % PCL:0.4 % chitosan	*Avg. fibre diameter* (nm): 404.0 ±207.8
REF: Rf-containing electrospun fibres, Rf = 14.3 wt%	Electrospun PCL/chitosan nanofibrous mesh with Rf PCL:chitosan:Rf = 60:6:11 = 4 % PCL:0.4 % chitosan:0.7 % Rf	*Avg. fibre diameter* (nm): 397.4 ±106.8
EFRM: electrospun fibres + Rf-containing micro-patterns, Rf = 14.3 wt%	Electrospun PCL/chitosan fibre mesh with PLGA/Rf micro-patterns PLGA:Rf = 6:1 = 6 % PLGA:1 % Rf	*Avg. fibre diameter* (nm): 404.0 ±207.8 *Avg. micropattern* (μm): 75.2 ±3.0

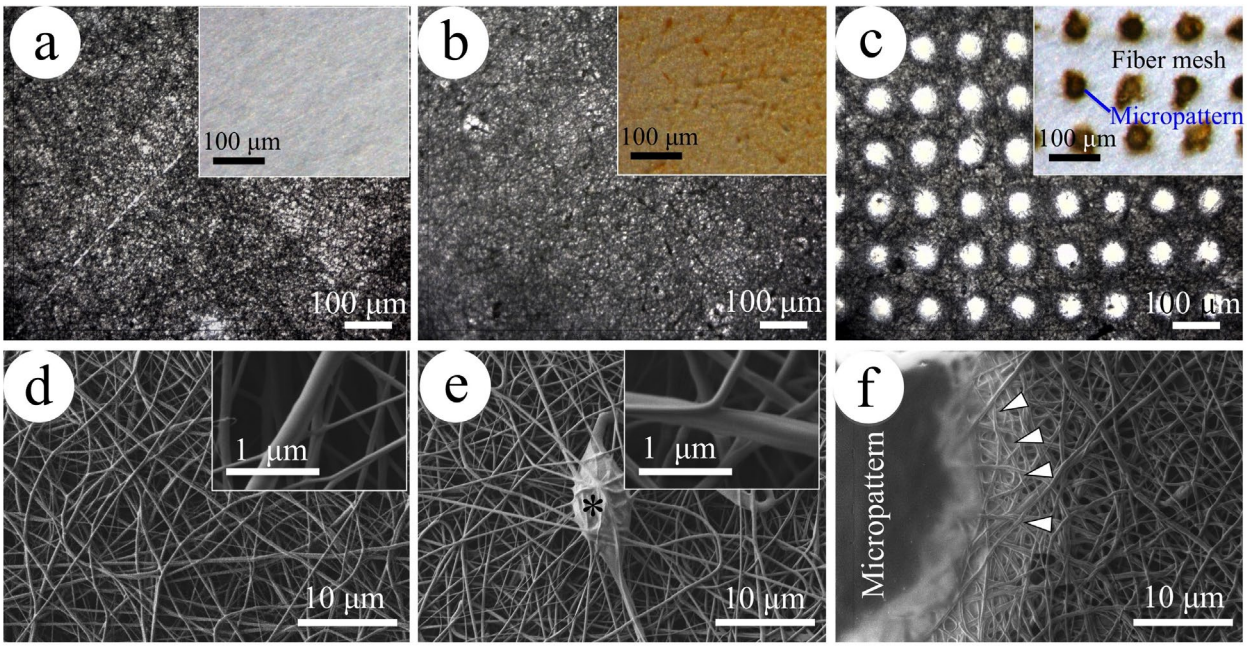

Fig. 2. Representative microscopic images of multifunctional biomimetic surfaces: EF (**a, d**), REF (**b, e**), and EFRM (**c, f**). Phase contrast optical images showed the surface morphology of various meshes and 50 µm PLGA micro-patterns (**a-c**) and stereo microscopic images showed the colour of Rf-containing nanofibres and PLGA micro-patterns (**a-c** inset). Scanning electron microscopic images showed the morphology of PCL/chitosan nanofibres (**d**), Rf-incorporating nanofibres (**e**) and the PLGA micro-patterns (**f**) and high magnification (d and e inset). Asterisk in (**e**): beads formed during electrospinning. Arrows in (**f**): the bonding between micro-patterns and nanofibres. (**a-c**) and their insets: Scale bar = 100 µm; (**d-f**): scale bar = 10 µm and their insets: scale bar = 1 µm.

ring and at 1545 cm^{-1} that corresponded to the stretching amide bond (Silverstein and Webster 1997) were observed on REF but not on EF meshes (Fig. 3). The deposition of Rf-containing micro-patterns, composed of arrays of dried Rf/PLGA droplets with ~75 µm in diameter (Fig. 2c and inset), onto PCL/chitosan nanofibre meshes did not affect the nanofibre morphology, while a tight bonding formed between the micro-patterns and the nanofibres (Fig. 2f).

Controlled release of Rf

The release of Rf from either REF or EFRM was performed in PBS (pH 7.0) at 37 °C for up to three days with Rf-free EF as controls (n = 3). With a similar release pattern, i.e., an initial burst release and cumulative release over a period of three days, a faster release rate was measured in REF compared to EFRM (Fig. 4). After one-hour incubation, about 71.9 % of the initially loaded Rf was released from REF, reaching 14.8 µg/mL in the supernatant. In comparison, about 41.7 % of the initially loaded Rf was released from EFRM for a concentration of 8.6 µg/mL in the supernatant. After 24 h, all Rf was released from REF, while 3.3 % Rf still remained in the PLGA micro-patterns of EFRM and was completely released in another 24 h. In both groups, the cumulatively released Rf drastically exceeded the minimal bactericidal concentration (MBC, 0.5 µg/mL) (Monzon *et al.,* 2001), sufficient to kill those *S. epidermidis* coming to the implant surface.

Bacterial culture

After 5 h bacterial culture, crystal violet staining showed that EF gave the most intense staining and EFRM the

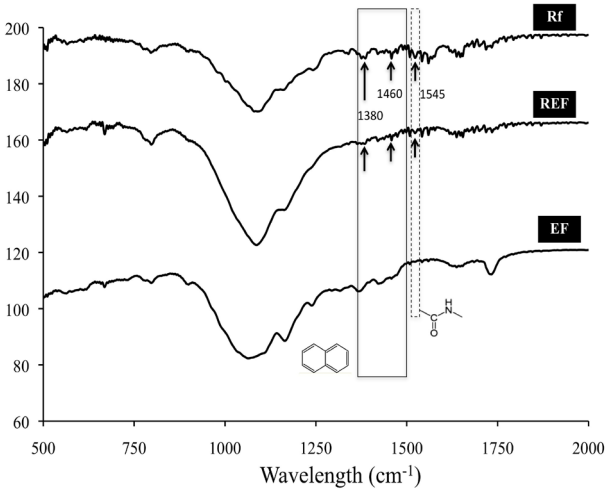

Fig. 3. Fourier transform infrared (FTIR) spectra of Rf, EF and REF.

lowest one, and there was no significant difference between EFRM and REF (Fig. 5a). Quantification of the staining by measuring the OD value of the extracts of crystal violet staining (n = 3) confirmed this observation, showing that the EF group stained approximately 6 times more than the REF group and 9 times more than the EFRM group (Fig. 5b). Close examination of the staining revealed the presence of only individual *S. epidermidis* cells in both REF and EFRM groups (white arrows in Fig. 5e and f insets) in contrast to large purple clumps in the EF group (asterisk of Fig. 5d inset). The fluorescent live/dead

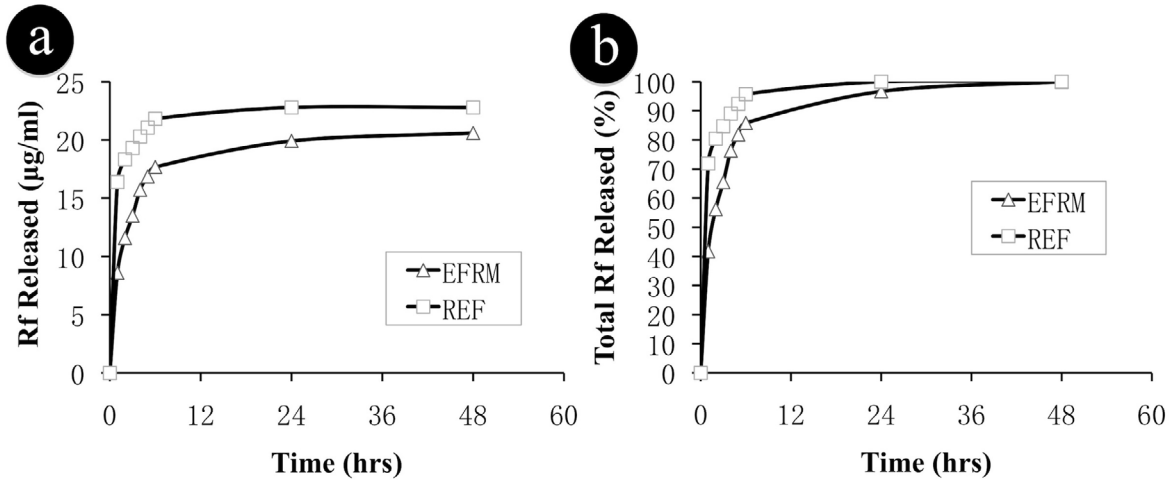

Fig. 4. Time-dependent release of Rf from REF or EFRM. Accumulative Rf concentration in the releasing buffer solution (**a**). Released RF as percentage of a total loaded (**b**).

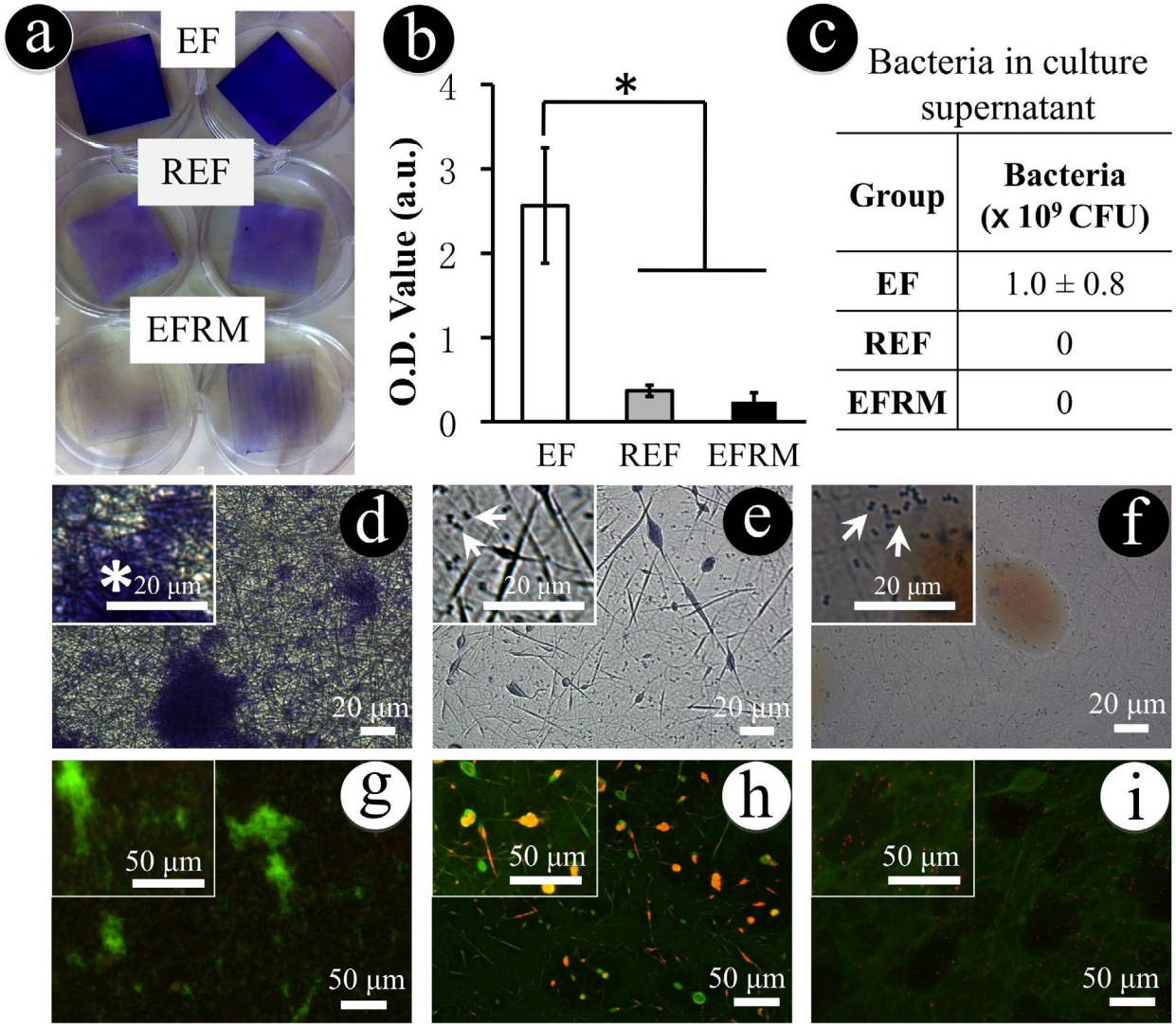

Fig. 5. Antibacterial activity of multifunctional surfaces. Representative optical images of various surfaces cultured with *S. epidermidis* for 5 hours and then stained with crystal violet (**a**). Quantification of the crystal violet-stained culture by measuring the optical density of the extracts (**b**). Quantification of *S. epidermidis* in the culture supernatants on various surfaces by agar plating (**c**). Optical images of various surfaces after crystal violet staining (**d-f**) and inset: high magnification. Asterisk in (**d**): bacterial mass; arrows in (**e**) and (**f**): individual bacterial cells. Fluorescent microscopic images of various surfaces after live/dead staining of the cultured *S. epidermidis* (**g-i**) and inset: high magnification. Green: live bacteria; red: dead bacteria. EF (**d, g**); REF (**e, h**); EFRM (**f, i**). * Statistically significant, $p < 0.01$. (**d-f**) Scale bar = 20 μm; (**g-i**) scale bar = 50 μm.

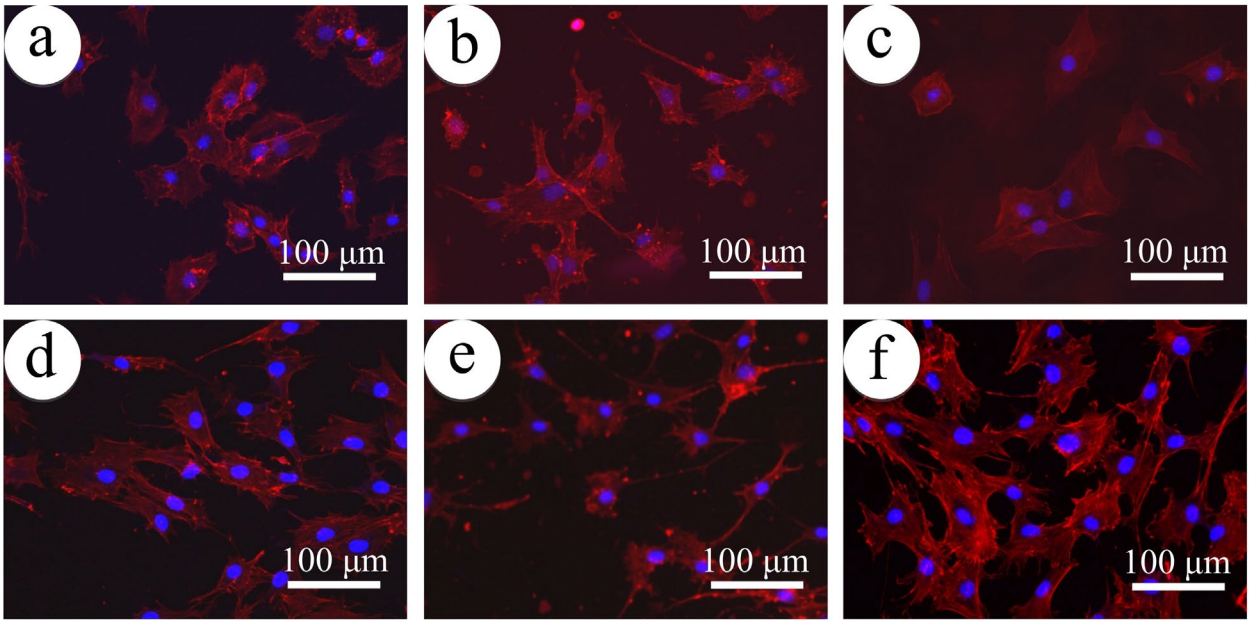

Fig. 6. Representative fluorescent images of mouse preosteoblasts cultured on various surfaces after 1 (**a-c**) and 3 days (**d-f**): EF (**a, d**), REF (**b, e**) and EFRM (**c, f**). The cells were stained with phalloidin-TRITC for F-actin (red) and DAPI for cell nuclei (blue). Scale bar = 100 µm.

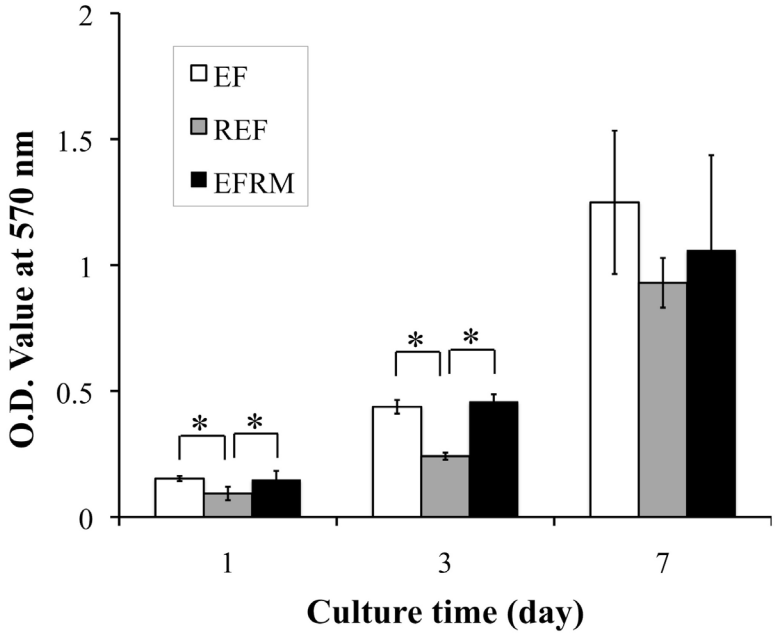

Fig. 7. Metabolic activity of mouse preosteoblasts on various surfaces determined by MTT assay. Data presented from three individual experiments. * Statistically significant, $p < 0.01$.

staining showed that only dead bacteria were detected in either REF or EFRM (red dots in Fig. 5h and i insets), while the large clump in EF controls contained a great quantity of live *S. epidermidis* as indicated by the intense green fluorescence in Fig. 5g. It is necessary to point out that the large and irregular fluorescent dots in Fig. 5h were artefacts from the beads formed during the electrospinning. The result of the agar-plating assay showed that no planktonic *S. epidermidis* was found in the supernatants of both REF and EFRM, while approximately 1.0×10^9 CFU/mL *S. epidermidis* was detected from the Rf-free EF controls (Fig. 5c).

Preosteoblast culture

The fluorescent staining of the cellular cytoskeleton filament actin (F-actin) showed that distinct cell morphology was noticed among various substrates as early as day 1. On both EF and EFRM, preosteoblasts began to adhere and spread in a polygonal morphology (Fig. 6a and c), while a constrained yet slim morphology (Fig. 6b) was consistently observed on the REF substrates even after 3-day culture (Fig. 6e). No noticeable difference could be identified between EF and EFRM. The MTT results ($n = 3$) showed that a significantly lower cell metabolic activity was measured in REF group at day 1 and 3, in comparison to both EF and EFRM groups ($p < 0.01$), and the difference became less obvious by 7 days after media change. Consistent with the fluorescent staining result, cell metabolic activity between EF and EFRM was comparable at all the investigated time points (Fig. 7).

The RT-PCR results ($n = 3$) showed that no significant difference was found in OPN expression among all three

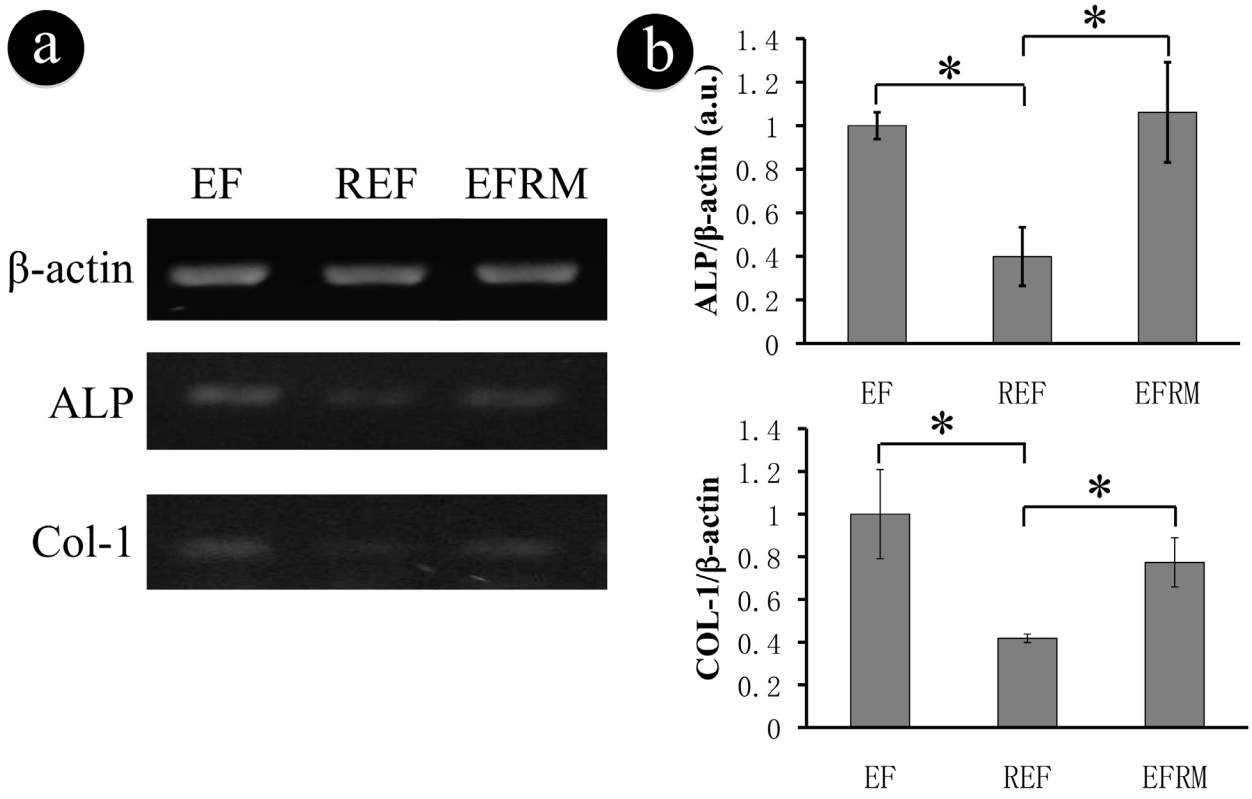

Fig. 8. Gene expression of osteogenic markers on various substrates (EF, REF and EFRM). Representative electrophoresis gel (**a**) and semi-quantitative analysis of gene expression (**b**). The data presented were normalised with β-actin. * Statistically significant, $p < 0.01$.

groups (data not shown), however, the expression of both type I collagen (COL-1) and alkaline phosphatise (ALP) was noticeably lower on the REF substrates (Fig. 8a) and semi-quantification of the expression intensity confirmed this observation (Fig. 8b). No significant difference between EF and EFRM was measured in both ALP and COL-1 gene expression (Fig. 8).

Discussion

The failure of long-term orthopaedic implants has mainly resulted from bacterial infection and implant loosening due to poor adhesion to host bone tissue (Van de Belt *et al*., 2001; Neut *et al.,* 2003; Campoccia *et al.,* 2006), so the intrinsic competition between infectious bacteria and tissue-forming cells for implant surface determines the benefits to design a cell-adhesive, bacteria-repulsive surface. Multistep efforts were made to modify the titanium surface with covalently grafted chitosan, hyaluronic acid or their derivatives to suppress bacterial adhesion, and immobilise RGD peptide or growth factors to enhance osseointegration (Shi *et al.,* 2008; Shi *et al.,* 2009; Hu *et al.,* 2010). However, these approaches involved not only two main chemical modification steps, but also several preparing and cleaning steps, which could potentially complicate its application by requiring a longer time and more chemicals to modify the titanium surface. In this regard, the present study was aimed to develop a simple and cost-effective strategy for modifying the implant surface with a similar multi-functionality and meanwhile applicability to a wider range of long-term orthopaedic implant substrates. Compared to previous efforts, the new approach only needed two steps, i.e., electrospinning and micro-pattern printing, which could be completed in several hours with a few economical chemicals. Thus, this approach can be readily translated into "clinically appropriate large scale production techniques" (Ozkan *et al.*, 2009) with reproducibility and cost-effectiveness.

The advantages of electrospun PCL/chitosan nanofibres (EF) in promoting bone cell adhesion and differentiation have been highlighted as a result of their morphological similarity to native ECM fibrils and the presence of chitosan (Yang *et al.,* 2009a). However, high bacterial adhesion to such nanofibrous meshes was also observed in the present study (Fig. 5a) and as reported previously (Wang *et al.,* 2010). To address this challenge, the incorporation of antibiotics into nanofibres seems to be a plausible solution (Zeng *et al*., 2003; Liang *et al.,* 2007; Sill and von Recum, 2008). By electrospinning the blended solutions containing a model antibiotic, Rf, Rf-containing PCL/chitosan nanofibres with a similar diameter to pure PCL/chitosan nanofibres (Fig. 2d and 2e, Table 1) were produced. Theoretically, the lipophilic nature of Rf (Zeng *et al*., 2003) would allow a complete dissolution of Rf in the PCL/chitosan solution to form a homogeneous blended solution and therefore produce the nanofibres with evenly distributed Rf. Indeed, most of the Rf distributed

uniformly across the PCL/chitosan nanofibre surface and it was confirmed by using a fluorescent substitute with comparable molecular weight, rhodamine 610 (Exciton, Dayton, OH, USA) (data not shown). However, a few large beads in dark red were also observed among the nanofibres (Fig. 2b inset and 2e). This may be ascribed to the possible binding of anionic RF with cationic chitosan to form complexes (Cao and Sun, 2009), which reduced the solution viscosity from 5.3×10^{-2} (PCL/chitosan) to 4.9×10^{-2} kg m^{-1} s^{-1} (PCL/chitosan/Rf) and affected the electrospinning process (Pham *et al.,* 2006). The high surface area/volume ratio of nanofibres allowed a rapid release of Rf (Fig. 4), consistent with our previous observation with BSA release (Yang and Wang, 2010). Additionally, during electrospinning the fast solvent evaporation and the high ionic strength of Rf in the solution might lead to the distribution of Rf mainly on the surface of PCL/chitosan fibres (Fig. 2b), which consequently causes an initial burst release of Rf (Zeng *et al.* 2003; Kim *et al.,* 2004; He *et al.,* 2009).

Rapid release of Rf from PCL/chitosan fibres results in a high Rf concentration in the culture sufficient to kill *S. epidermidis* and prevent biofilm formation. Indeed, only individual *S. epidermidis* bacteria were observed in the Rf-containing nanofibres (Fig. 5e) and a majority of them were stained dead (Fig. 5h). It is necessary to mention that Rf may not be the best choice, however, it demonstrates its effectiveness as a model antibiotic to kill planktonic *S. epidermidis* of NJ9709 strain in this study, i.e., where it was incorporated into PCL/chitosan nanofibres (REF) or PLGA micro-patterns (EFRM), and it can be easily replaced with a better one or a cocktail due to the flexibility of our approach. Our previous study has shown a negligible toxicity of Rf to osteoblasts even up to 60 μg/mL (Lee *et al.*, 2011), which is about two times higher than the maximum Rf concentration (i.e., 22.8 μg/mL) released from REF or EFRM in this study. However, the homogeneous distribution of RF across PCL/chitosan nanofibres could change the surface properties of nanofibres (Fig. 3). Clearly, variation in surface properties would modulate the interactions between electrospun nanofibres and cell membrane integrin receptors (Huang *et al.,* 2008; Tambralli *et al.,* 2009; Kwei *et al.,* 2010), which are closely associated with intracellular signalling, and therefore affects the cell metabolic activity and differentiation (Giancotti, 1999; Schwartz and Assoian, 2001). Indeed, the attachment and spreading of preosteoblasts on REF were noticeably different from those on EF (Fig. 6). Significantly lower cell metabolic activity was measured on REF for up to 3 days compared to EF meshes. Since Rf was completely released from the nanofibres after two days (Fig. 4), no Rf was left in the fibres after medium change on day 3. As a result, the difference in cell metabolic activity on day 7 became less pronounced among all three groups (Fig. 7), further suggesting the unfavourable effect of Rf presented in the PCL/chitosan nanofibres. Similar results were also consistently observed with other tissue cells such as fibroblasts (data not shown). Moreover, it was confirmed that the presence of Rf in the PCL/chitosan nanofibres decreased the expression of osteogenic markers (Fig. 8).

To minimise the detrimental influence of Rf to the surface properties of PCL/chitosan nanofibres, it is possible to encapsulate Rf in the core to form core-shell nanofibres *via* coaxial electrospinning (Sun *et al.,* 2003; Jiang *et al.*, 2005; Zhang *et al.,* 2007). However, prolonged processing and narrow drug loading capacity could be a challenge in adopting this technique, apart from the need of special setups (Maretschek *et al.,* 2008).

Deposition of Rf-eluting PLGA micro-patterns on PCL/chitosan nanofibre meshes allows the incorporation of Rf onto the nanofibre substrate without changing the surface properties (Fig. 2). Different from the uniform distribution of Rf in REF fibres, Rf in PLGA micro-patterns disperses as discrete particles of ~10-100 nm (Gu *et al.*, 2012) as a result of the re-crystallisation of Rf with slow evaporation of DMSO during ink-jet patterning. The distinct appearance of Rf in REF and PLGA micro-patterns of EFRM probably contributes partially to the differential release profile of Rf as shown in Fig. 4. In addition, the slower Rf release from EFRM may also come from the fact that Rf particles were effectively embedded in PLGA micro-patterns and its release would greatly depend on the degradation kinetics of the PLGA matrix (Polakovic *et al.*, 1999; Commandeur *et al.*, 2006; Gu *et al.*, 2012). In this regard, it is possible to decelerate the Rf release rate by utilising less hydrophilic PLGA or increasing the molecular weight of PLGA (Murakami *et al.*, 2000). Although a slower Rf release rate was measured from the EFRM substrates (about 58.0 % of REF in 1 h), sufficient Rf was released within the first hour (much higher than MBC of 0.5 μg/mL) to eradicate *S. epidermidis* and stunt biofilm formation. Earlier studies have demonstrated the necessity of rapidly releasing antibiotics within a few hours after surgery to efficiently eliminate the bacteria before they begin to proliferate (Bölgen *et al.*, 2007; He *et al.*, 2009; Yoo *et al.*, 2009). The culture of preosteoblasts on EFRM substrates did not adversely affect the cellular response, and instead followed a similar pattern to those on the EF controls in terms of cell spreading, proliferation and differentiation (Fig. 6-8). The possible explanations to this are (1) the 75 μm Rf-containing PLGA micro-pattern arrays deposited on the nanofibre meshes only take about 20 % of the total surface area, and (2) the 150 μm inter-micro-pattern distance is large enough for the preosteoblasts to attach, spread and proliferate onto the intact PCL/chitosan nanofibre surfaces. Considering that only one micro-pattern configuration was used in this study, our further efforts will focus on addressing whether reduced micro-pattern separation distances can affect the behaviour of preosteoblasts.

In this study, the effort to integrate biomimetic nanofibres with antibiotic-eluting micro-patterns for possible modification of orthopaedic implant surfaces was the first attempt to minimise infection and promote bone tissue formation. With the successful demonstration of the dual function, our continuous efforts will focus on the integration of such fibre meshes to implant surface. Interestingly, our initial measurement has shown a good bonding force between electrospun nanofibre meshes and smooth titanium alloy ($TiAl_6V_4$) substrates (the roughness is ~0.05 μm) (data not shown), close to the strength of human bone (~18 MPa) (Kar *et al.,* 2006), suggesting its

good resistance to mechanical disruption and potential use for implant surface. Furthermore, its application can also be extended to other possibilities, e.g., to modify other types of long-term implants by choosing appropriate nanofibres and drugs or to be used as wound dressing and surgical meshes.

Conclusions

For those long-term orthopaedic implants, the design of a multifunctional surface to minimise infection while supporting tissue formation represents a promising paradigm. In recognition of the stimulatory effect of PCL/chitosan biomimetic nanofibres on tissue formation, the incorporation of antibiotics (e.g., Rf) to nanofibre meshes for infection control may achieve the desired multi-functionality. In this study, deposition of Rf-containing PLGA micro-patterns (~75 μm in diameter and ~150 μm apart) onto PCL/chitosan electrospun nanofibres yield a multifunctional substrate, which can effectively kill *S. epidermidis* and prevent biofilm formation without sacrificing the osteogenic properties of PCL/chitosan nanofibres. Taken together, the present study provides further evidence to the emerging efforts in designing multi-functional surfaces for enhancing bone tissue formation while controlling infection.

Acknowledgements

This investigation was sponsored by the Biomedical Engineering and Biomaterials program of the National Science Foundation (CBET 1033742 and DMR 1005902). Xuening Chen is also partially supported by Innovation & Entrepreneurship Doctoral Fellowship from Stevens Institute of Technology.

References

Alt V, Bitschnau A, Osterling J, Sewing A, Meyer C, Kraus R, Meissner SA, Wenisch S, Domann E, Schnettler R (2006) The effects of combined gentamicin-hydroxyapatite coating for cementless joint prostheses on the reduction of infection rates in a rabbit infection prophylaxis model. Biomaterials **27**: 4627-4634.

Banerjee I, Ravindra CP, Ravi SK (2011) Antifouling coatings: recent developments in the design of surfaces that prevent fouling by proteins, bacteria, and marine organisms. Adv Mater **23**: 690-718.

Bearinger JP, Terrettaz S, Michel R, Tirelli N, Vogel H, Textor M, Hubbell JA (2003) Chemisorbed poly (propylene sulphide)-based copolymers resist biomolecular interactions. Nat Mater **2**: 259-264.

Bölgen N, Vargel I, Korkusuz P, Menceloğlu YZ, Pişkin E (2007) *In vivo* performance of antibiotic embedded electrospun PCL membranes for prevention of abdominal adhesions. J Biomed Mater Res B: Appl Biomater **81**: 530-543.

Campoccia D, Lucio M, Arciola CR (2006) The significance of infection related to orthopedic devices and issues of antibiotic resistance. Biomaterials **27**: 2331-2339.

Cao Z, Sun Y (2009) Chitosan-based rechargeable long-term antimicrobial and biofilm-controlling systems. J Biomed Mater Res A 89: 960-967.

Commandeur S, van Beusekom HM, van der Giessen WJ (2006) Polymers, drug release, and drug-eluting stents. J Intervent Cardiol **19**: 500-506.

Giancotti FG (1999) Integrin signaling. Science **285**: 1028-1033.

Gristina AG (1987) Biomaterial-centered infection: Microbial adhesion *versus* tissue integration. Science **237**: 1588-1595.

Gu YX, Chen XN, Lee JH, Monteiro DA, Wang HJ, Lee WY (2012) Inkjet-printed antibiotic- and calcium-eluting bioresorbable nanocomposite micro-patterns for orthopaedic implants. Acta Biomater **8**: 424-431.

Hamade RF, Zeineddine F, Akle B, Smaili A (2005) Modelangelo: a subtractive 5-axis robotic arm for rapid prototyping. Robotics Computer-Integr Manufact **21**: 133-144.

Hayes JS, Vos DI, Hahn J, Pearce SG, Richards RG (2009) An *in vivo* evaluation of surface polishing of Tan intermedullary nails for ease of removal. Eur Cell Mater **18**: 15-26.

Hayes JS, Seidenglanz U, Pearce AI, Pearce SG, Archer CW, Richards RG (2010) Surface polishing positively influences ease of plate and screw removal. Eur Cell Mater **19**: 117-126.

Hayes JS, Welton JL, Wieling R, Richards RG (2012) *In vivo* evaluation of defined polished titanium surfaces to prevent soft tissue adhesion. Journal of Biomedical Materials Research Part B, Applied Biomater **100**: 611-617.

He CL, Huang ZM, Han XJ (2009) Fabrication of drug-loaded electrospun aligned fibrous threads for suture applications. J Biomed Mater Res A **89**: 80-95.

Hu XF, Neoh KG, Shi ZL, Kang ET, Poh C, Wang W (2010) An *in vitro* assessment of titanium functionalized with polysaccharides conjugated with vascular endothelial growth factor for enhanced osseointegration and inhibition of bacterial adhesion. Biomaterials **31**: 8854-8863.

Huang C, Fu X, Liu J, Qi Y, Li S, Wang H (2012) The involvement of integrin β1 signaling in the migration and myofibroblastic differentiation of skin fibroblasts on anisotropic collagen-containing nanofibers. Biomaterials **33**: 1791-1800.

Huang Z, Sargeant TD, Hulvat JF, Mata A Jr, Pablo B, Koh C, Stupp SI, Snead ML (2008) Bioactive nanofibers instruct cells to proliferate and differentiate during enamel regeneration. J Bone Miner Res **23**: 1995-2006.

Jiang HL, Hu YQ, Li Y, Zhao PC, Zhu KJ, Chen WL (2005) A facile technique to prepare biodegradable coaxial electrospun nanofibers for controlled release of bioactive agents. J Control Rel **108**: 237-243.

Kaplan JB, Ragunath C, Velliyagounder K, Fine DH, Ramasubbu N (2004) Enzymatic detachment of Staphylococcus epidermidis biofilms. Antimicrob Agents Chemother **48**: 2633-2636.

Kar A, Raja KS, Misra M (2006) Electrodeposition of hydroxyapatite onto nanotubular TiO2 for implant applications. Surf Coat Technol **201**: 3723-3731.

Katti DS, Robinson KW, Ko FK, Laurencin CT (2004) Bioresorbable nanofiber-based systems for wound healing

and drug delivery: optimization of fabrication parameters. J Biomed Mater Res B: Applied Biomater **70**: 286-296.

Kenawy E, Bowlin GL, Mansfield K, Layman J, Simpson DG, Sanders EH, Wnek GE (2002) Release of tetracycline hydrochloride from electrospun poly(ethylene-co-vinylacetate), poly(lactic acid), and a blend. J Control Rel **81**: 57-64.

Kim K, Luu YK, Chang C, Fang DF, Hsiao BS, Chu B, Hadjiargyrou M (2004) Incorporation and controlled release of a hydrophilic antibiotic using poly(lactide-co-glycolide)-based electrospun nanofibrous scaffolds. J Control Rel **98**: 47-56.

Kwei SP, Moffat KL, Levine WN, Lu HH (2010) Nanofiber alignment regulates adhesion and integrin expression of human mesenchymal stem cells and tendon fibroblasts. Proc 2010 IEEE 36th Ann Northeast Bioeng Conf (NEBEC) **14**: 1-2.

Lee JH, Kaplan JB, Lee WY (2011) Microfluidic approach to create 3D tissue models biofilm related infection of orthopaedic implants. Tissue Eng C Meth **17**: 39-48.

Liang DH, Hsiao BS, Chu B (2007) Functional electrospun nanofibrous scaffolds for biomedical applications. Adv Drug Del Rev **59**: 1392-1412.

Lucke M (2003) Gentamicin coating of metallic implants reduces implant-related osteomyelitis in rats. Bone **32**: 521-531.

Maretschek S, Greiner A, Kissel T (2008) Electrospun biodegradable nanofiber nonwovens for controlled release of proteins. J Control Rel **127**: 180-187.

Monzon M, Oteiza C, Leiva J, Amorena B (2001) Synergy of different antibiotic combinations in biofilms of Staphylococcus epidermidis. J Antimicrob Chemother **48**:793-801.

Moriarty TF, Debefve L, Boure L, Campoccia D, Schlegel U, Richards RG (2009) Influence of material and microtopography on the development of local infection *in vivo*: experimental investigation in rabbits. Int J Artific Org **32**: 663-670.

Moriarty TF, Campoccia D, Nees SK, Boure LP, Richards RG (2010) *In vivo* evaluation of the effect of intramedullary nail microtopography on the development of local infection in rabbits. Int J Artific Org **33**: 667-675.

Murakami H, Kobayashi M, Takeuchi H, Kawashima Y (2000) Utilization of poly(DL-lactide-co-glycolide) nanoparticles for preparation of mini-depot tablets by direct compression. J Control Rel **67**: 29-36.

Neut D, van Horn JR, van Kooten TG, van der Mei HC and Busscher HJ (2003) Detection of biomaterial-associated infections in orthopaedic joint implants. Clin Orthopaed Rel Res **413**: 261-268.

O'Reilly T, Kunz S, Sande E, Zak O, Sande MA, Tauber MG (1992) Relationship between antibiotic concentration in bone and efficacy of treatment of staphylococcal osteomyelitis in rats: azithromycin compared with clindamycin and rifampin. Antimicrob Agents Chemother **36**: 2693-2697.

Otto DP, Vosloo HC, Liebenberg W, de Villiers MM (2008) Development of microporous drug-releasing films cast from artificial nanosized latexes of poly(styrene-co-methyl methacrylate) or poly(styrene-co-ethyl methacrylate). Eur J Pharm Biopharm **69**: 1121-1134.

Ozkan S, Kalyon DM, Yu XJ, Mckelvey CA, Lowinger M (2009) Multifunctional protein-encapsulated polycaprolactone scaffolds: Fabrication and *in vitro* assessment for tissue engineering. Biomaterials **30**: 4336-4347.

Pham QP, Sharma U and Mikos AG (2006) Electrospinning of polymeric nanofibers for tissue engineering application: a review. Tissue Eng **12**: 1197-1211.

Polakovic M, Gorner T, Gref R, Dellacherie E (1999) Lidocaine loaded biodegradable nanospheres. II. Modelling of drug release. J Control Rel **60**: 169-177.

Radin S, Ducheyne P (2007) Controlled release of vancomycin from thin sol-gel films on titanium alloy fracture plate material. Biomaterials **28**: 1721-1729.

Schindler M, Ahmed I, Kamal J, Nur-E-Kamal A, Grafe TH, Chung HY, Meiners S (2005) A synthetic nanofibrillar matrix promotes *in vivo*-like organization and morphogenesis for cells in culture. Biomaterials **26**: 5624-5631.

Schwartz MA, Assoian RK (2001) Integrins and cell proliferation: regulation of cyclin-dependent kinases *via* cytoplasmic signaling pathways. J Cell Sci **114**: 2553-2560.

Shasha B, Lang R, Rubinstein E (1994) Efficacy of combinations of doxycycline and rifampicin in the therapy of experimental mouse brucellosis. J Antimicrob Chemother **33**: 545-551.

Shi ZL, Neoh KG, Kang ET, Poh C, Wang W (2008) Bacterial adhesion and osteoblast function on titanium with surface-grafte chitosan and immobilized RGD peptide. J Biomed Mater Res A **86**: 865-872.

Shi ZL, Neoh KG, Kang ET, Poh C, Wang W (2009) Surface functionalization of titanium with carboxymethyl chitosan and immobilized bone morphogenetic protein-2 for enhanced osseointegration. Biomacromolecules **10**: 1603-1611.

Sieuwerts AM, Klijn JG, Peters HA, Foekens JA (1995) The MTT tetrazolium salt assay scrutinised: how to use this assay reliably to measure metabolic activity of cell cultures *in vitro* for the assessment of growth characteristics, IC50-values and cell survival. Eur J Clin Chem Clin Biochem **33**: 813-823.

Sill TJ, von Recum HA (2008) Electrospinning: applications in drug delivery and tissue engineering. Biomaterials **29**: 1989-2006.

Silverstein RM, Webster FX (1997) Spectrometric Identification of Organic Compounds, 6th Ed. John Wiley & Sons, Hoboken, NJ, pp 101.

Sun Z, Zussman E, Yarin AL, Wendorff JH, Greiner A (2003) Compound Core–Shell Polymer Nanofibers by Co-Electrospinning. Adv Mater **15**: 1929-1932.

Tambralli A, Blakeney B, Anderson J, Kushwaha M, Andukuri A, Dean D, Jun HW (2009) A hybrid biomimetic scaffold composed of electrospun polycaprolactone nanofibers and self-assembled peptide amphiphile nanofibers. Biofabrication **1**: 025001.

van de Belt H, Neut D, Schenk W, van Horn JR, van der Mei HC, Busscher HJ (2001) Infection of orthopedic

implants and the use of antibiotic-loaded bone cements. A review. Acta Orthopaed Scand **72**: 557-571.

Venugopal JR, Zhang Y, Ramakrishna S (2006) *In vitro* culture of human dermal fibroblasts on electrospun polycaprolactone collagen nanofibrous membrane. Artif Org **30**: 440-446.

Wang C, Yang F, Zhang H (2010) Fabrication of non-woven composite membrane by chitosan coating for resisting the adsorption of proteins and the adhesion of bacteria. Separ Purif Technol **75**: 358-365.

Yang XC, Wang HJ (2010) Electrospun functional nanofibrous scaffolds for tissue engineering. In: Tissue Engineering (Eberli D, ed), Intech, New York, pp 159-178,

Yang XC, Chen XN, Wang HJ (2009a) Acceleration of osteogenic differentiation of preosteoblastic cells by chitosan containing nanofibrous scaffolds. Biomacromolecules **10**: 2772-2778.

Yang XC, Shah JD, Wang HJ (2009b) Nanofiber enabled layer-by-layer approach toward three-dimensional tissue formation. Tissue Eng A **15**: 945-956.

Yin Z, Chen X, Chen JL, Shen WL, Nguyen TMH, Gao L, Ouyang HW (2010) The regulation of tendon stem cell differentiation by the alignment of nanofibers. Biomaterials **31**: 2163-2175.

Yoo HS, Kim TG, Park TG (2009) Surface-functionalized electrospun nanofibers for tissue engineering and drug delivery. Adv Drug Del Rev **61**: 1033-1042.

Zeng J, Xu XY, Chen XS, Liang QZ, Bian XC, Yang LX, Jing XB (2003) Biodegradable electrospun fibers for drug delivery. J Control Rel **92**: 227-231.

Zhang YZ, Su B, Venugopal J, Ramakrishna S, Lim CT (2007) Biomimetic and bioactive nanofibrous scaffolds from electrospun composite nanofibers. Int J Nanomedicine **1**: 623-638.

Zimmerli W, Widmer AF, Blatter M, Frei R, Ochsner PE (1998) Role of rifampin for treatment of orthopedic implant-related staphylococcal infections. J Am Med Ass **279**: 1537-1541.

Zimmerli W, Trampuz A, Ochsner PE (2004) Prosthetic-joint infections. N Engl J Med **351**:1645-1654.

Zong X, Li S, Chen E, Garlick B, Kim KS, Fang D, Chiu J, Zimmerman T, Brathwaite C, Hsiao BS, Chu B (2004) Prevention of postsurgery-induced abdominal adhesions by electrospun bio- absorbable nanofibrous poly(lactide-co-glycolide)-based membranes. Ann Surg **240**: 910-925.

Discussion with Reviewers

Reviewer I: Can the authors extend on the possible use of these meshes?

Authors: Yes. Although in this study nanofibre meshes with antibiotic-eluting micro-patterns are primarily used to modify the orthopaedic implant surfaces for minimising infection and promoting bone tissue formation, their application can be extended to other possibilities, e.g., to modify other types of implants by choosing the appropriate nanofibres and drugs or to be used as wound dressing and surgical meshes.

Reviewer II: How would you compare the findings of your study to other methods for creating a functionalised surface? What are the potential advantages and disadvantages of your proposed method compared to other described methods?

Authors: Considering the primary objective of this study to achieve a dual functional surface, i.e., preventing infection while promoting osteogenesis, printing of antibiotic-eluting PLGA micro-patterns onto PCL/chitosan nanofibre meshes proves to be effective in eliminating the model *S. epidermidis* strain without sacrificing the osteogenic feature of PCL/chitosan nanofibres. Actually, this strategy has the flexibility to choose a single or a cocktail of antibiotics to be included in the micro-patterns and to configure the biomimetic nanofibres to be tissue specific. Compared to those efforts in modifying the surface either for infection control or for tissue formation (Bearinger *et al.,* 2003; Alt *et al.,* 2006; Banerjee *et al.,* 2011, text references), clearly the dual functions as addressed would be superior. Additionally, this approach is rather straightforward and cost-effective, overcoming the technical challenge and complexity confronted with chemical modification of the surfaces, which quite often is surface specific (Shi *et al.,* 2008; Shi *et al.,* 2009; He *et al.,* 2010, text references). Meanwhile, this method can be applied to a wide range of implant substrates and has the potential to be used as wound dressing and surgical meshes depending on the mechanical strength of fibre meshes.

Reviewer III: In the introduction the authors mention that more cost-effective approaches are preferred. Can they explain why the nanofibres in combination with printed pattern will be more cost effective than other methods?

Authors: Nanofibres have shown their advantages in promoting cell adhesion and spreading, which may limit the need of growth factors or cytokines. Meanwhile, the simple setup and low cost to fabricate nanofibres *via* electrospinning represent another promising dimension for rapid translation to application. Incorporation of antibiotics into PLGA micro-patterns allows precise control of the amount of antibiotics for delivery by manipulating the size of micro-patterns and the inter-micro-pattern distance. In addition, a low amount of antibiotics is needed for local delivery compared to systematic administration. Compared to other efforts to produce multifunctional surfaces, e.g., functionalisation of titanium substrates with covalently grafted chitosan, hyaluronic acid or their derivatives for suppressing bacterial adhesion, and with immobilised RGD or growth factors for enhancing osseointegration (Hu *et al*., 2010; Shi *et al*., 2008; Shi *et al*., 2009, text references), which always require more steps (chemical modification and rinsing steps) and longer preparation time (a few days), the reported approach simply composes two steps (electrospinning and printing) and can be completed within a few hours. The simplified operations may allow the use of robotics to further improve the efficiency and lower the cost.